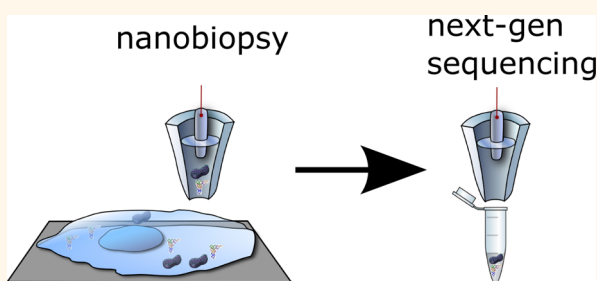


Compartmental Genomics in Living Cells Revealed by Single-Cell Nanobiopsy

Paolo Actis,^{†,§} Michelle M. Maalouf,[§] Hyunsung John Kim, Akshar Lohith, Boaz Vilozny, R. Adam Seger, and Nader Pourmand*

Department of Biomolecular Engineering, University of California Santa Cruz, 1156 High Street, Santa Cruz, California 95064, United States. [§]These authors contributed equally. [†]Present address: Department of Medicine, Imperial College London, Du Cane Road, London W12 0NN, United Kingdom.

ABSTRACT The ability to study the molecular biology of living single cells in heterogeneous cell populations is essential for next generation analysis of cellular circuitry and function. Here, we developed a single-cell nanobiopsy platform based on scanning ion conductance microscopy (SICM) for continuous sampling of intracellular content from individual cells. The nanobiopsy platform uses electrowetting within a nanopipette to extract cellular material from living cells with minimal disruption of the cellular milieu. We demonstrate the subcellular resolution of the nanobiopsy platform by isolating small subpopulations of mitochondria from single living cells, and quantify mutant mitochondrial genomes in those single cells with high throughput sequencing technology. These findings may provide the foundation for dynamic subcellular genomic analysis.



KEYWORDS: nanopipette · scanning ion conductance microscopy · single-cell biopsy · electrowetting · mitochondria · next-generation sequencing

Most tissues in the body consist of a fine architecture of cells with sub-structural mosaics of cell clusters and intricate yet ill-defined circuits. Cells interact with other cells to produce precise functioning of tissues, organs, and organ systems. Understanding the molecular biology of individual cells within circuits in complex environments is necessary to understand both normal physiology and also how injury or disease causes pathology to alter cell function.¹

Furthermore, investigations into the molecular basis of cancer cell transformation, proliferation, and metastasis would be aided by technologies capable of analysis of molecules and genetic factors involved in disease progression at a single cell level. This is particularly true for cancer because tumors are heterogeneous and consist of cells at different stages of transformation. Studies on whole tissue provide only a statistical average of the many events occurring in different cells. Single cell analysis may reveal how tumorigenesis-related signaling pathways can cause genetic changes which ultimately lead to the

transformation of a healthy cell to a cancerous cell.

Anatomical approaches have been employed for a century to study tissue architecture and cellular heterogeneity and have provided insights into cell–cell interaction and circuitry within tissues. However, these approaches are usually employed post-mortem, reducing our ability to study the dynamic function of individual cells in heterogeneous populations. Also, much of what we know of individual cell molecular biology in our body is diluted by analysis of mixed cellular populations in heterogeneous tissues.

Attempts to study single cell molecular biology in heterogeneous tissue cultures began several decades ago when patch-clamp approaches were used to isolate RNA from neurons to profile the gene expression of single cells² linking genetics to neuronal function.³ This approach provided only a snapshot of single cell molecular biology, because once the neuron was impaled by the micropipet it died. Over the last 20 years, other approaches have been employed to study single cell molecular

* Address correspondence to pourmand@soe.ucsc.edu.

Received for review October 1, 2013 and accepted November 26, 2013.

Published online November 26, 2013
10.1021/nn405097u

© 2013 American Chemical Society

biology, including laser capture microdissection techniques.⁴ Again, these approaches either study cells postmortem, which prevents analysis of dynamic changes in the cell's genomics over time, or they do not maintain the natural environment of a cell in heterogeneous tissues.

Nanoscale devices are ideal single-cell surgical tools because of their potential for high spatial and temporal resolution studies.^{5–8} Recently, two groups independently developed cellular nanoendoscopes for single cell analysis. Singhal *et al.*⁹ attached a carbon nanotube to the tip of a glass micropipet and showed its potential for interrogating cells by transporting fluids and performing optical and electrochemical diagnostics down to the single organelle level. Similarly, Yan *et al.*¹⁰ developed a nanowire waveguide attached to the tip of an optical fiber, which can transmit visible light into intracellular compartments of a living mammalian cell and detect optical signals from subcellular regions. The cylindrical shape of these nanoendoscopes allows the probing of organelles deep inside the cell.

Integration of nanoendoscopes with scanning probe techniques may allow automation and high-throughput analysis. In 2003, Osada and co-workers inserted atomic force microscope (AFM) tips into living cells to extract mRNAs which were then analyzed with PCR techniques.¹¹ More recently, Wickramasinghe's group optimized this method by coating AFM tips with platinum, allowing extraction of the mRNA molecules through dielectrophoresis. Wickramasinghe's technology has been successfully combined with standard assay techniques to detect RNA molecules in breast cancer cells.^{12,13}

Scanning ion conductance microscopy (SICM) is a scanning probe technique that has recently gained attention for its ability to image living cells with high spatial¹⁴ and temporal resolution.¹⁵ SICM relies on a glass nanopipette filled with an electrolyte solution biased to generate an ion flow through the nanopipette aperture.^{16,17} The nanopipette is then scanned over a surface and changes in the magnitude of the measured ion current reflect the topography of the sample.^{18,19} Nanopipettes have been recently utilized to measure the electrophysiology at small synaptic boutons,²⁰ to locally deliver molecules to multiple subcellular areas,²¹ and to trap molecules in lipid bilayers.²² Our group has developed nanopipettes as a label-free sensing platform,^{23–28} and we recently described an adaptation of SICM allowing the multi-component injection of single cells in culture.²⁹ Laforge *et al.*³⁰ developed an electrochemical attosyringe based on a glass nanopipette to deliver a minute amount of liquid into a living cell *via* electrowetting. Briefly, when a nanopipette is filled with an organic solution and immersed into an aqueous one, a liquid–liquid interface is formed at the nanopipette opening. If a voltage is then applied across this

interface, a force is generated that can induce the aqueous solution to flow into/out of the nanopipette.³¹

To begin to study the molecular properties of living cells, we adapted an SICM platform that uses electrowetting within a nanopipette to extract minute quantities of cellular material from living cells in culture with minimal disruption and combine it with sensitive sequencing technologies to study the genomics of individual cells and their organelles.

RESULTS AND DISCUSSION

Nanopipettes were integrated into a custom-built scanning ion conductance microscope (SICM) (Figure 1a) that allows automated positioning of the nanopipette nanometers above the cell.²⁹ To adapt the SICM as a single-cell biopsy platform, the nanopipette was filled with a 10 mM THATPBCl solution in DCE, and fitted with a silver wire coated with AgTBACl (see online methods). When a DCE-filled nanopipette is immersed into an aqueous solution, a liquid–liquid interface is formed at the nanopore lumen due to the hydrophobic nature of DCE.^{32,33} The application of a voltage across this interface induces a change in the DCE surface tension. This effect, called electrowetting, causes the aqueous solution to flow in the nanopipette when a negative voltage is applied and to flow out when the bias is reversed (Supporting Information, Figures 2 and 3 and Video 1). From geometrical calculations this volume was estimated to be ~ 50 fL, which corresponds to $\sim 1\%$ of the volume of a cell.

While in cell culture medium, the nanopipette is polarized with a positive bias to prevent medium from flowing into the barrel. This bias generates an ion current through the liquid–liquid interface which is used as the input into a feedback loop. Custom-designed software directs the nanopipette toward the cell until it detects a 0.5% drop in the ionic current. At this point the software stops the approach and quickly lowers the nanopipette by $1 \mu\text{m}$ at a high speed ($100 \mu\text{m/s}$) to pierce the cell membrane (Figure 1b), inserting the nanopipette tip into the cell cytoplasm. The nanopipette bias is then switched to -500 mV for 5 s, which causes the controlled influx of cell cytoplasm into the nanopipette (Figure 1b,c) followed by a switch to 100 mV, which stops the influx but does not cause the efflux of aspirated contents. The nanopipette is then quickly raised, and the aspirated content is transferred into a $5 \mu\text{L}$ droplet of RNase-free H_2O by application of $+1$ V for 2 min and kept at 4°C .

Because of the small pore of the nanopipette (50 nm in radius), its insertion into cells is minimally invasive (Figure 2a, Supporting Information, Figure 1). This is a major advance over previous approaches for single cell molecular analysis, which employed micropipets that severely damage cell membranes. As a result, the nanopipette technology can be used to sample living cells multiple times in the life of a cell to study

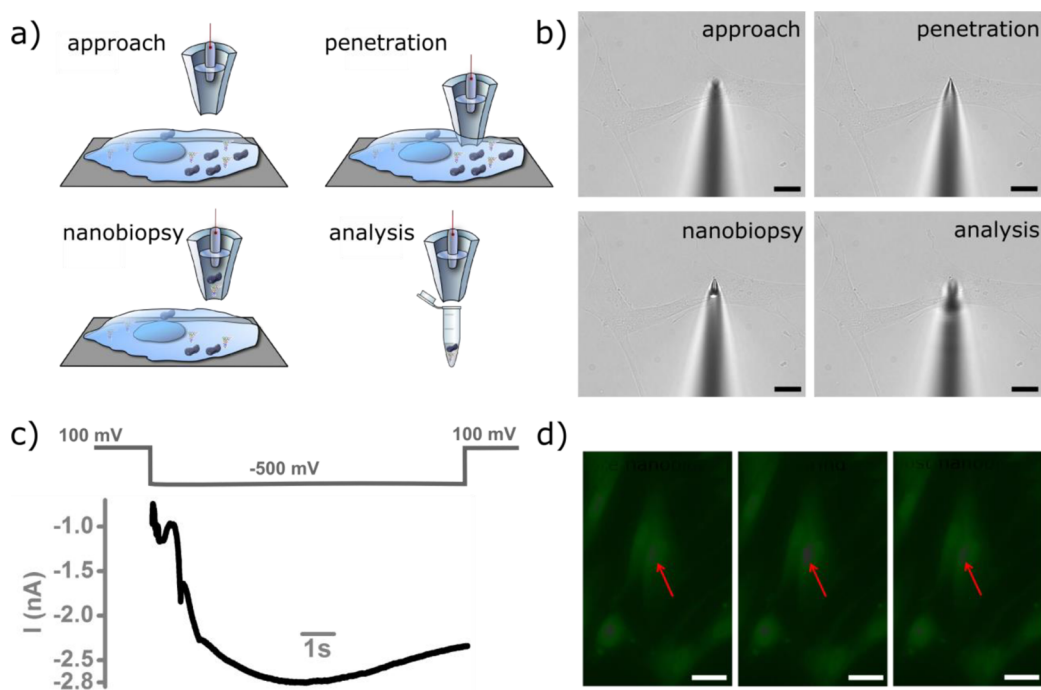


Figure 1. Schematic of single cell nanobiopsy. (a) Illustration of automated approach to cell surface, penetration in the cell cytosol, followed by controlled aspiration of cytoplasmic material by electrojetting, and delivery of the biopsied material into a tube for analysis. Scheme not to scale. (b) Optical micrographs of the nanobiopsy procedure illustrating the approach, cell membrane penetration, aspiration *via* electrojetting, and retraction of the nanopipette tip. Scale bars 25 μm . (c) Chronoamperometry during nanobiopsy. A nanopipette filled with a 10 mM solution of THATPBCl penetrates a cell in culture. Before the penetration, the nanopipette is biased at +100 mV to prevent any aqueous solution from entering into the tip. After cell membrane penetration, the bias is switched to -500 mV. The entry of intracellular solution in the nanopipette tip causes the ion current to increase. (d) Calcium imaging during nanobiopsy procedure showing false color fluorescent micrographs of human BJ fibroblast cells stained with Fluo4 AM during nanobiopsy. Red arrows indicate where the nanopipette penetrated the cell. Scale bars 25 μm .

molecular dynamics. To show the effect of the nanopipette on cell function is innocuous, human BJ fibroblast cells were loaded with the Ca^{2+} imaging agent Fluo4 AM and fluorescent microscopy was used to measure localized intracellular $[\text{Ca}^{2+}]$ before, during, and after the nanobiopsy (Figure 1d). Optical micrographs confirm that the procedure is minimally invasive, generating a barely detectable Ca^{2+} change during nanobiopsy. The cell fully recovers within 5 s postaspiration, reaching $[\text{Ca}^{2+}]$ that matches the pre-aspiration level. In contrast, cellular biopsy using micropipets employed for patch clamp electrophysiology show dramatic changes in cytosolic Ca^{2+} concentration in the cell (Supporting Information, Figure 7). Because the nanopipette is minimally invasive, it can be employed for multiple samplings of cellular cytoplasm without overtly altering cell function. The 100-nm diameter of the nanopipettes limits the interaction of DCE with the cell membrane to an area of $\sim 0.01 \mu\text{m}^2$. This area is about 0.004% of the total surface area of a cell in culture (assuming the surface area of cell being equal to $\sim 250 \mu\text{m}^2$). The disruption to the cell function is mainly caused by the aspiration of cellular contents and the application of a potential through the cell membrane. Furthermore, we performed cell viability studies that indicated a survival rate higher

than 70% for the 50+ nanobiopsies performed in this study.

To validate the nanobiopsy platform, small cytoplasmic samples were isolated from single HeLa cells expressing GFP, and PCR was used to amplify GFP transcripts (Figure 2a,b). The total RNA was reverse-transcribed to generate cDNA, and real time-PCR analysis of cDNA confirmed the presence of GFP transcripts (see Supporting Information). The real-time PCR amplification plots show a C_q value of 20 for the positive control (total RNA extracted from ~ 10000 HeLa-GFP cells), 30 when the input RNA was the biopsied content of a single cell, and 33 for the negative control (water). The difference in C_q values from the positive control and biopsied sample is 10, which corresponds to a 2^{10} -fold (1024 fold) difference in input material (Figure 2b).

Because individual cells are known to have variability in gene expression, the reproducibility of the nanobiopsy protocols was tested by performing aspiration in a solution containing the lysate of ~ 10000 GFP HeLa cells. Nanobiopsy (Figure 2c, blue curve) represents the average with error bars of four nanobiopsies performed with four different nanopipettes in a PBS solution containing the lysate of ~ 10000 GFP HeLa cells. Postaspiration analysis *via* qPCR (Figure 2c)

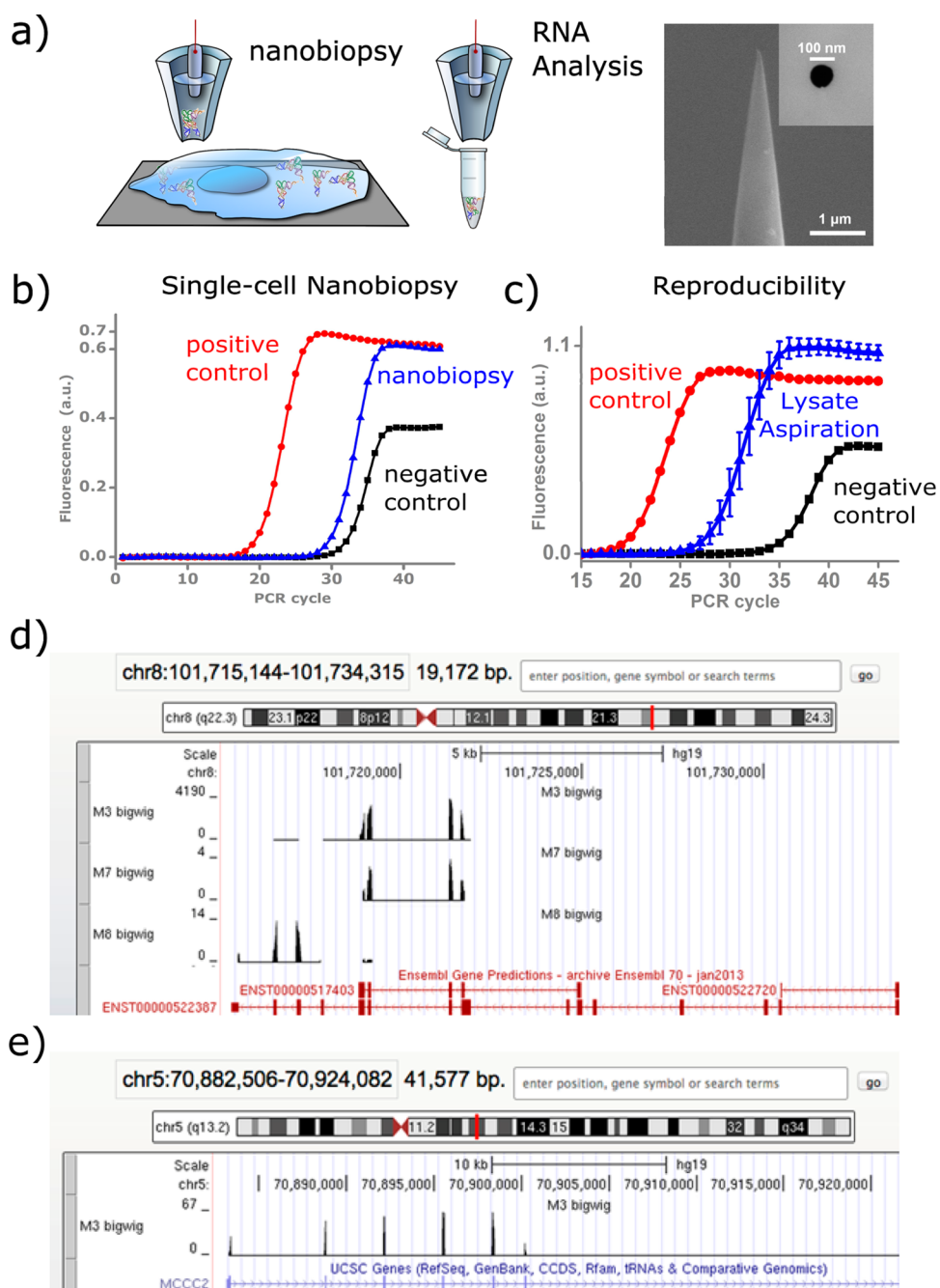


Figure 2. RNA analysis post-nanobiopsy. (a) Scheme not to scale showing nanobiopsy followed by RNA analysis and SEM micrograph of a representative nanopipette tip. (b) Postbiopsy analysis *via* qPCR targeting GFP RNA from HeLa cells showing a positive control of total RNA from a ~ 1000 cells lysate (red curve, $C_q = 20$), a nanobiopsy taken from within a single cell (blue curve, $C_q = 30$) and the negative control (black curve, $C_q = 33$). (c) Reproducibility of nanobiopsy protocols. qPCR targeting GFP RNA. Positive control (red curve) consists of RNA extracted for GFP HeLa cells spiked in the cDNA synthesis mix. Nanobiopsy (blue curve) represents the average of four nanobiopsies with four different nanopipettes performed in a PBS solution containing the lysate of ~ 10000 GFP HeLa cells following the protocol described in the manuscript. Negative control (black curve) where no input material was used for cDNA synthesis. (d,e) Read coverage of RNA sequencing of aspirations are displayed in the UCSC genome browser. Genomic position is displayed along the X axis and depth of coverage is represented in the Y axis. (d) Ensemble gene predictions are displayed in red, where lines represent introns and rectangles represent exons. These gene predictions are on the reverse strand and are displayed in the 3' to 5' direction. Alternative 3' exon usage in the gene PABPC1 is seen in M3 and M7 vs M8. M8 shows coverage over the 3' region of the longer isoform, whereas M3 and M7 show coverage over the shorter isoform. (e) The gene MCCC2 is displayed in blue in the 5' to 3' direction. Read coverage extends across the entire length of the gene and demonstrates the feasibility of generating full length cDNA from transcripts isolated by nanobiopsy.

confirmed the high reproducibility of the nanobiopsy protocols. Overall, out of the 50+ nanobiopsies performed in this study we obtained a success rate of 70%

for RNA aspirations, as confirmed by PCR analysis followed by gel electrophoresis (Supporting Information, Figure 6).

In addition to qPCR analysis, cDNA of mature mRNA was generated, sequenced and the reads mapped to the human reference genome (see Supporting Information). Differential 3' untranslated region (UTR) usage in cytoplasmic Poly-A binding protein (PABPC1) was observed, where two aspirations show dominant expression of a noncanonical isoform, whereas the third shows expression of the canonical isoform (Figure 2d). We have also observed instances where coverage was obtained over an entire transcript rather than just the 3' UTR. An example of read coverage over the full length of methylcrotonoyl-CoA carboxylase 2 (MCCC2) is shown in Figure 2e.³⁴ These results demonstrate the feasibility of generating mRNA expression from single living cells using the nanobiopsy platform. Finally, when enriched for the most overrepresented Gene Ontologies, we found that two aspirations predominantly expressed machinery related to translation, while one was enriched for processes related to metabolism and morphogenesis demonstrating that nanobiopsy can be used to analyze endogenous RNAs.

In addition to total RNA analysis of a cell, the nanobiopsy platform can be employed to isolate and analyze cellular organelles, specifically mitochondria. Mitochondria are essential for energy production and express their own genome distinct from the nuclear genome, providing a way to establish the subcellular resolution of the nanopipette technique.

To show that it was possible to isolate mitochondria from a cell and study the mitochondria genome independently of the nuclear genome, human BJ fibroblasts were stained using MitoTracker Green (Invitrogen) (Figure 3a, Supporting Information, Figure 8), a fluorescent label for mitochondria. The nanopipette was placed above a region of the cell with an abundance of mitochondria, and a biopsy was taken (Figure 3a right panel). Fluorescence within the tip of the nanopipette indicated the successful aspiration of mitochondria (Figure 3b right panel).

Next-generation sequencing was employed to sequence the genomes of the biopsied mitochondria. The mitochondrial DNA was amplified using primers specific to the mitochondrial genome. This approach is novel and important because it allows us to selectively sequence the mitochondrial genome without the need to separate the mitochondrial nucleic acids from the more abundant nuclear DNA. The amplified mitochondrial DNA was subjected to gel electrophoresis which revealed that all three samples show bands at the correct length for human mitochondrial DNA (Supporting Information, Figure 9).

The nanobiopsy relies on the voltage-controlled aspiration of cellular material and not on adsorption to the nanopipette side walls. No amplification is observed if a negative voltage is not applied to the nanopipette after insertion into the cell and when aspiration is performed in the bulk solution

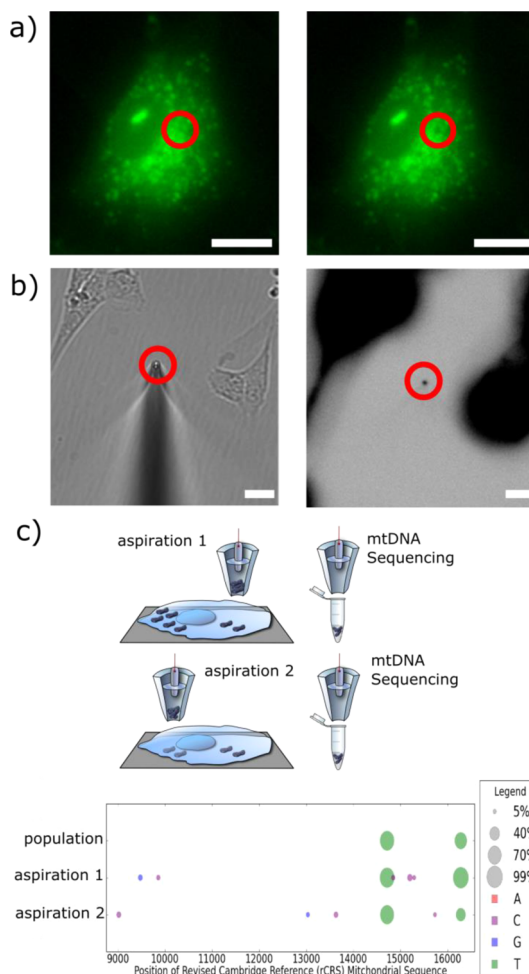


Figure 3. Mitochondrial nanobiopsy. (a) Fluorescent micrograph of human BJ fibroblast cells stained with MitoTracker Green before nanobiopsy (right panel) and after nanobiopsy (left panel). Red circles highlight a dark spot caused by mitochondria removal. Scale bars 15 μm . (b) (left panel) Bright-field image of the nanopipette tip (red circle) used for mitochondria nanobiopsy in panel a. (Right panel) Negative fluorescent micrograph (black areas indicate high fluorescence) of left panel showing fluorescence arising from the nanopipette tip which indicates the success of mitochondria nanobiopsy. Scale bars 15 μm . (c) Sequencing results demonstrate variable conservation of heteroplasmic frequencies in aspirations. Heteroplasmic variants with estimated frequencies between 5% and 99% are displayed as circles where the area of the circle is proportional to the observed frequency. The nucleotide of the variant is specified by the color, where "A" is represented in red, "C" is represented in violet, "G" is represented in blue, and "T" is represented in green. The 14713 A \rightarrow T variant shows similar frequencies across aspirations and population; whereas the 16278 C \rightarrow T variant shows a greater variance of heteroplasmic frequencies in aspirations. Low frequency variants were also found in both aspirations but not in the population.

(Supporting Information, Figure 4). This is the key element that differentiates the nanobiopsy technology from AFM-based platforms. Both Wickramasinghe's and Osada's groups used AFM probes to extract RNA from cells in culture, either based on physisorption or hybridization of complementary RNA immobilized onto the probe.^{11,12} By contrast, the hollow nature of

nanopipette probes allows general fluid aspiration, thus its application is not limited to nucleic acid.

Sequencing results from two mitochondria aspirations from a single cell, as well as DNA extracted from a population of cells revealed that the frequencies of some heteroplasmic variants are more conserved at the subcellular level (Figure 3c). For example, two heteroplasmic variants (14713 A→T and 16278 C→T) were found both in subcellular aspirations and samples from the total (pooled) mitochondrial population. Frequencies of the 14713 A→T variant were found to be similar across all samples, 83%, 87%, and 79%. However, the 16278 C→T variant showed substantial variation in frequencies with 62%, 98%, and 38% frequencies for the pooled versus the selected mitochondria, respectively. Whereas the average heteroplasmic frequency is observable in population-based sequencing, only subcellular sequencing revealed heterogeneity of the variant within a cell. On the basis of the genomic data of the pooled mitochondrial population data alone, it would be impossible to know that the frequency of the 16278 C→T variant fluctuated more than the 14713 A→T variant, despite similar representation in the population. The 16278 C→T variant represents a common polymorphism occurring in 1845 out of 16411 mitochondrial sequences in Genbank. Although this particular variant does not appear to have any disease function, mitochondrial DNA mutations have been implicated in tumorigenesis. Tracking the emergency of somatic variants could help elucidate mechanisms by which cancers escape cell death and increase proliferation

In addition to the differences in heteroplasmic frequencies among subcellular aspirations, we were also able to detect a number of variants that were >5% of sequencing reads. We were able to detect five variants between 5 and 15% in Aspiration 2 and four variants in Aspiration 1 (*p*-value <0.005 in both cases). These very rare variants were not detectable in the total

mitochondrial population sample and may represent variants within individual mitochondrial genomes. These results show that by a combination of the nanopipette with a novel mitochondrial directed genomic technology, small subpopulations of mitochondrial genomes in single cells can be sequenced.

CONCLUSIONS

We have developed a minimally invasive nanosurgical technology to interrogate living cells. Minute amounts of total RNA and mitochondrial DNA were taken out of a single cell and nucleic acids were analyzed using next generation genomic sequencing techniques. Current methods for single-cell manipulation often can detect only one class of analytes. For example, it is possible to isolate total cellular RNA to conduct mRNA profiling in single cells. In contrast, the nanobiopsy platform has subcellular resolution and can be used to isolate small subpopulations of mitochondria from single living cells, and quantify mutant mitochondrial genomes in those single cells with high throughput DNA/RNA sequencing technology. As a consequence, mitochondrial mutation rates can be assessed in single cells, a key step in interrogating why and how cellular degenerative mutations gradually build up over time to cause cellular dysfunction and death. The use of nanopipettes to aspirate just a few copies of mitochondrial DNA from a living cell might provide the basis for less invasive and more accurate monitoring of disease progression, or lay the foundation for developing new classes of drugs to attenuate neurodegeneration or to treat diseases as diverse as Parkinson's Disease, and Alzheimer's Disease. The nanopipettes can be used as a platform in cancer research and clinical management, elucidating the role of heterogeneity in primary tumor tissues and systemically identifying critical parameters in disease progression and potential metastatic states.^{35–38}

MATERIALS AND METHODS

Electrowetting in Nanopipettes. Nanopipettes were fabricated from quartz capillaries (Sutter Instrument, Novato, CA) using a P-2000 laser puller (Sutter Instrument, Novato, CA). Mean diameter = (106 ± 16) nm (Supporting Information, Figure 1). Quartz nanopipettes were filled with a solution of 1,2-dichloroethane (DCE) containing 10 mM tetrahexylammonium tetrakis(4-chlorophenyl)borate (THATPBCL). A silver wire coated with silver tetrakis(4-chlorophenyl)borate (AgTBACl) was then inserted into the barrel of the nanopipette, while a Ag/AgCl wire was immersed in the bath solution acting as a reference/counter electrode.

SICM setup. The scanning ion conductance microscope (SICM) consists of a Axopatch 200B low-noise amplifier (Molecular Devices, Sunnyvale, CA) for nanopipette bias and current measurement, a MP-285 micromanipulator (Sutter Instrument, Novato, CA) for coarse control in the X, Y, and Z directions, a Nanocube piezo actuator (Physik Instrumente, Irvine, CA) for fine control in the X, Y, and Z directions, and a PCIe-7851R Field Programmable Gate Array

(FPGA) (National Instruments) for hardware control of the system. The system is operated using custom coded software written in LabVIEW.⁸

Cell Culture. BJ Human Fibroblasts were purchased from Stemgent and cultured in Stromal Cell Basal Medium (SCBM) (Lonza, Alpharetta, GA) with supplements (Lonza, Alpharetta, GA) with no phenol-red. HeLa cells (Cell Biolabs, San Diego, CA) expressing Green Fluorescent Protein were cultured in 70% DMEM medium supplemented with 10% fetal bovine serum, 0.1 mM essential amino acids, 2 mM L-glutamine, and 1% Pen-Strep as suggested from the supplier. All cells were cultured in 5% CO₂ at 37 °C. Cells were plated on both ungridded and gridded plates (ibidi, μ -Dish35 mm, highGrid-500 uncoated, sterile) coated with 1% gelatin. Cells were plated at about 5×10^4 cells per dish.

cDNA Synthesize and qPCR. cDNA was synthesized from total RNA nanobiopsied from cells using iScript cDNA Synthesis Kit (BioRad, Hercules, CA) following manufacturer recommendations. Quantitative PCR (qPCR) was used to confirm the success

of the nanobiopsy protocols using Clontech's Advantage qPCR Premix SYBR Green I Master Mix (Clontech, Mountain View, CA) following manufacturer recommendations. PCR primers: HeLa-GFP, Reverse primer: GCGCCGAGGTGAAGTTCGAGG, Forward Primer: GCCGTCCCGATGGGGGTGT were used to amplify the aspirated mitochondrial DNA to amplify 3968 base pairs visualized by gel electrophoresis.

cDNA Synthesis and RNA Sequencing. Aspirated RNA samples were processed to cDNA using the Ovation RNA-Seq system (NuGEN Technologies, San Carlos, CA). The cDNA was prepared for individual aspiration for library preparation. The quality and quantity of single-cell cDNA were evaluated using the Agilent Bioanalyzer 2100 DNA High Sensitivity chip (Agilent, Palo Alto, CA).

For paired-end whole transcriptome library preparation, *ca.* 0.5–1.0 μ g cDNA of each sample was sheared to a size ranging between 200 and 300 bp using the Covaris-S2 sonicator (Covaris, Woburn, MA) according to the manufacturer's recommended protocols. Fragmented cDNA samples were used for the preparation of RNA-Seq libraries using TruSeq v1 Multiplex sample preparation kit (Illumina, San Diego, CA). Briefly, cDNA fragments were end repaired, dA-tailed, and ligated to multiplex adapters according to manufacturer's instructions. After ligation, DNA fragments smaller than 150 bp were removed with AmPure XP beads (Beckman Coulter Genomics, Danvers, MA). The purified adapter-ligated products were enriched using polymerase chain reaction (14 cycles). The final amplified libraries were resolved on 2.0% agarose gel and size-selected in the range of 350–380 bp using the Caliper XT system (PerkinElmer, Waltham, MA). The final RNA-Seq libraries were quantitated using the Agilent bioanalyzer 2100 and pooled together in equal concentration for sequencing. The pooled multiplexed libraries were sequenced and generated 2 \times 150 bp paired-end reads on MiSeq (Illumina, San Diego, CA).

Mitochondrial DNA Amplification and Sequencing. Aspirated mitochondrial DNA was amplified by long and accurate PCR using a pair of primers; forward TCA TTT TTA TTG CCA CAA CTA ACC TCC TCG GAC TC and reverse CGT GAT GTC TTA TTT AAG GGG AAC GTG TGG GCT AT to generate a \sim 8K bp fragment. The aspirated mitochondrial genomes were amplified using long and accurate polymerase chain reaction (LA-PCR) LA PCR Kit ver. 2.1 (Takara Bio). The mitochondrial genome amplification was carried out in a 25 μ L reaction mixture containing aspirated template DNA, 2.5 μ L of 10X Epicenter's boost, 2.5 μ L of 10X LA PCR buffer II (Mg²⁺ plus), 4.0 μ L of dNTP (2.5 mM), 1.25 μ L of each primer (10 μ M), 0.125 μ L of LA Taq DNA Polymerase, and 11.4 μ L of sterile distilled water. Thermocycler conditions were 95 $^{\circ}$ C for 2 min, followed by 30 cycles, each consisting of 94 $^{\circ}$ C for 15 s then 68 $^{\circ}$ C for 8 min, and a final extension at 68 $^{\circ}$ C for 13 min. The mitochondrial amplicons were sheared by Covaris S2 systems resulting in 300–400 bp fragments that were subjected to automated Illumina multiplex paired end library preparation on robot. A unique index sequence was used for each mitochondrial sample and sequenced in a single Illumina HiSeq 2000 lane.

Bioinformatics Methods. Short reads from mitochondrial experiments were preprocessed to trim sequencing adapters from the 3' ends of reads. Mitochondrial reads were aligned to the revised Cambridge Mitochondrial Reference Sequence using a nonspliced aligner. Heteroplasmic variants between 5% and 99% were reported. Short reads from RNA-sequencing experiments were preprocessed to trim sequencing adapters from the 3' ends of reads. Ten bases from the 5' end of RNA-seq reads were processed to remove biases introduced during second strand synthesis of cDNA. RNA-seq reads were aligned to the hg19 UCSC human reference genome³⁴ and to UCSC known genes using a spliced alignment tool. Genes were considered expressed if at least one read mapped uniquely to an annotated transcript. Geneset enrichment analysis was performed on detected genes and overrepresented Gene Ontologies were reported. Detailed bioinformatics methodology is available in the Methodology section of the Supporting Information.

Conflict of Interest: The authors declare no competing financial interest.

Acknowledgment. We thank Prof. Holger Schmidt and Dr. Tom Yuzvinsky of the Keck Center for Nanoscale Optofluidics at UC Santa Cruz for electron microscopy of nanopipettes.

We thank Miten Jain and Brandon Rice for help in preliminary experiments. We thank Yidan Chen for technical assistance. This work was supported in part by grants from the National Cancer Institute [U54CA143803] and the National Institutes of Health [P01-35HG000205].

Supporting Information Available: SEM images of nanopipettes; electrochemical characterization of electrowetting in a nanopipette; THATPBCI salt synthesis; qPCR control experiments; calcium imaging during microbioopsy with a micropipette; gel electrophoresis showing reproducibility of nanobiopsy protocols (RNA and mitochondria); bioinformatics methods; video supplements. This material is available free of charge via the Internet at <http://pubs.acs.org>.

REFERENCES AND NOTES

- Schubert, C. Single-Cell Analysis: The Deepest Differences. *Nature* **2011**, *480*, 133–137.
- Van Gelder, R. N.; von Zastrow, M. E.; Yool, A.; Dement, W. C.; Barchas, J. D.; Eberwine, J. H. Amplified RNA Synthesized from Limited Quantities of Heterogeneous cDNA. *Proc. Natl. Acad. Sci.* **1990**, *87*, 1663–1667.
- Eberwine, J.; Bartfai, T. Single Cell Transcriptomics of Hypothalamic Warm Sensitive Neurons that Control Core Body Temperature and Fever Response: Signaling Asymmetry and an Extension of Chemical Neuroanatomy. *Pharmacol. Ther.* **2011**, *129*, 241–259.
- Emmert-Buck, M. R.; Bonner, R. F.; Smith, P. D.; Chuaqui, R. F.; Zhuang, Z.; Goldstein, S. R.; Weiss, R. A.; Liotta, L. A. Laser Capture Microdissection. *Science* **1996**, *274*, 998–1001.
- Tian, B.; Cohen-Karni, T.; Qing, Q.; Duan, X.; Xie, P.; Lieber, C. M. Three-Dimensional, Flexible Nanoscale Field-Effect Transistors as Localized Bioprobes. *Science* **2010**, *329*, 830–834.
- Yum, K.; Wang, N.; Yu, M.-F. Nanoneedle: A Multifunctional Tool for Biological Studies in Living Cells. *Nanoscale* **2010**, *2*, 363–372.
- Meister, A.; Gabi, M.; Behr, P.; Studer, P.; Vörös, J. N.; Niedermann, P.; Bitterli, J.; Polesel-Maris, J. R. M.; Liley, M.; Heinzelmann, H.; et al. FluidFM: Combining Atomic Force Microscopy and Nanofluidics in a Universal Liquid Delivery System for Single Cell Applications and Beyond. *Nano Lett.* **2009**, *9*, 2501–2507.
- Zheng, X. T.; Li, C. M. Single Living Cell Detection of Telomerase Over-Expression for Cancer Detection by an Optical Fiber Nanobiosensor. *Biosens. Bioelectron.* **2010**, *25*, 1548–1552.
- Singhal, R.; Orynbayeva, Z.; Kalyana Sundaram, R. V.; Niu, J. J.; Bhattacharyya, S.; Vitol, E. A.; Schrlau, M. G.; Papazoglou, E. S.; Friedman, G.; Gogotsi, Y. Multifunctional Carbon-Nanotube Cellular Endoscopes. *Nat. Nanotechnol.* **2011**, *6*, 57–64.
- Yan, R.; Park, J.-H.; Choi, Y.; Heo, C.-J.; Yang, S.-M.; Lee, L. P.; Yang, P. Nanowire-Based Single-Cell Endoscopy. *Nat. Nanotechnol.* **2012**, *7*, 191–196.
- Uehara, H.; Kunitomi, Y.; Ikai, A.; Osada, T. mRNA Detection of Individual Cells with the Single Cell Nanoprobe Method Compared with *In Situ* Hybridization. *J. Nanobiotechnol.* **2007**, *5*, 7.
- Nawarathna, D.; Chang, R.; Nelson, E.; Wickramasinghe, H. K. Targeted Messenger RNA Profiling of Transfected Breast Cancer Gene in a Living Cell. *Anal. Biochem.* **2011**, *408*, 342–344.
- Nawarathna, D.; Turan, T.; Wickramasinghe, H. K. Selective Probing of mRNA Expression Levels within a Living Cell. *Appl. Phys. Lett.* **2009**, *95*, 083117.
- Novak, P.; Li, C.; Shevchuk, A. I.; Stepanyan, R.; Caldwell, M.; Hughes, S.; Smart, T. G.; Gorelik, J.; Ostanin, V. P.; Lab, M. J.; et al. Nanoscale Live-Cell Imaging Using Hopping Probe Ion Conductance Microscopy. *Nat. Methods* **2009**, *6*, 279–281.
- Shevchuk, A. I.; Novak, P.; Taylor, M.; Diakonov, I. A.; Ziyadeh-Isleem, A.; Bitoun, M.; Guichenev, P.; Lab, M. J.; Gorelik, J.; Merrifield, C. J.; Klenerman, D.; Korchev, Y. E. An

- Alternative Mechanism of Clathrin-Coated Pit Closure Revealed by Ion Conductance Microscopy. *J. Cell Biol.* **2012**, *197*, 499–508.
16. Chen, C.-C.; Zhou, Y.; Baker, L. A. Scanning Ion Conductance Microscopy. *Annu. Rev. Anal. Chem.* **2012**, *5*, 207–228.
17. Rheinlaender, J.; Geisse, N. A.; Proksch, R.; Schäffer, T. E. Comparison of Scanning Ion Conductance Microscopy with Atomic Force Microscopy for Cell Imaging. *Langmuir* **2010**, *27*, 697–704.
18. Hansma, P.; Drake, B.; Marti, O.; Gould, S.; Prater, C. The Scanning Ion-Conductance Microscope. *Science* **1989**, *243*, 641–643.
19. Korchev, Y. E.; Bashford, C. L.; Milovanovic, M.; Vodyanoy, I.; Lab, M. J. Scanning Ion Conductance Microscopy of Living Cells. *Biophys. J.* **1997**, *73*, 653–658.
20. Novak, P.; Gorelik, J.; Vivekananda, U.; Shevchuk, Andrew I.; Ermolyuk, Yaroslav S.; Bailey, Russell J.; Bushby, Andrew J.; Moss, Guy W. J.; Rusakov, Dmitri A.; Klenerman, D.; *et al.* Nanoscale-Targeted Patch-Clamp Recordings of Functional Presynaptic Ion Channels. *Neuron* **2013**, *79*, 1067–1077.
21. Babakinejad, B.; Jönsson, P.; López Córdoba, A.; Actis, P.; Novak, P.; Takahashi, Y.; Shevchuk, A.; Anand, U.; Anand, P.; Drews, A.; *et al.* Local Delivery of Molecules from a Nanopipette for Quantitative Receptor Mapping on Live Cells. *Anal. Chem.* **2013**, *85*, 9333–9342.
22. Jönsson, P.; McColl, J.; Clarke, R. W.; Ostanin, V. P.; Jönsson, B.; Klenerman, D. Hydrodynamic Trapping of Molecules in Lipid Bilayers. *Proc. Natl. Acad. Sci.* **2012**, *109*, 10328–10333.
23. Actis, P.; Rogers, A.; Nivala, J.; Vilozny, B.; Seger, R. A.; Jejelowo, O.; Pourmand, N. Reversible Thrombin Detection by Aptamer Functionalized STING Sensors. *Biosens. Bioelectron.* **2011**, *26*, 4503–4507.
24. Umehara, S.; Karhanek, M.; Davis, R. W.; Pourmand, N. Label-Free Biosensing with Functionalized Nanopipette Probes. *Proc. Natl. Acad. Sci.* **2009**, *106*, 4611–4616.
25. Actis, P.; Jejelowo, O.; Pourmand, N. Ultrasensitive Mycotoxin Detection by STING Sensors. *Biosens. Bioelectron.* **2010**, *26*, 333–337.
26. Vilozny, B.; Wollenberg, A. L.; Actis, P.; Hwang, D.; Singaram, B.; Pourmand, N. Carbohydrate-Actuated Nanofluidic Diode: Switchable Current Rectification in a Nanopipette. *Nanoscale* **2013**, *5*, 9214–9221.
27. Vilozny, B.; Actis, P.; Seger, R. A.; Vallmajo-Martin, Q.; Pourmand, N. Reversible Cation Response with a Protein-Modified Nanopipette. *Anal. Chem.* **2011**, *83*, 6121–6126.
28. Actis, P.; Vilozny, B.; Seger, R. A.; Li, X.; Jejelowo, O.; Rinaudo, M.; Pourmand, N. Voltage-Controlled Metal Binding on Polyelectrolyte-Functionalized Nanopores. *Langmuir* **2011**, *27*, 6528–6533.
29. Adam Seger, R.; Actis, P.; Penfold, C.; Maalouf, M.; Vilozny, B.; Pourmand, N. Voltage Controlled Nano-Injection System for Single-Cell Surgery. *Nanoscale* **2012**, *4*, 5843–5846.
30. Laforge, F. O.; Carpino, J.; Rotenberg, S. A.; Mirkin, M. V. Electrochemical Attosyringe. *Proc. Natl. Acad. Sci.* **2007**, *104*, 11895–11900.
31. Dale, S. E. C.; Unwin, P. R. Polarised Liquid/Liquid Micro-Interfaces Move During Charge Transfer. *Electrochem. Commun.* **2008**, *10*, 723–726.
32. Liu, S.; Li, Q.; Shao, Y. Electrochemistry at Micro- and Nanoscopic Liquid/Liquid Interfaces. *Chem. Soc. Rev.* **2011**, *40*, 2236–2253.
33. Girault, H.; Schiffrin, D. Electrochemistry of Liquid–Liquid Interfaces. *Electroanal. Chem.* **1989**, *15*, 1–141.
34. Kent, W. J.; Sugnet, C. W.; Furey, T. S.; Roskin, K. M.; Pringle, T. H.; Zahler, A. M.; Haussler, David. The Human Genome Browser at UCSC. *Genome Res.* **2002**, *12*, 996–1006.
35. Clark, I. E.; Dodson, M. W.; Jiang, C.; Cao, J. H.; Huh, J. R.; Seol, J. H.; Yoo, S. J.; Hay, B. A.; Guo, M. *Drosophila Pink1* is Required for Mitochondrial Function and Interacts Genetically with *Parkin*. *Nature* **2006**, *441*, 1162–1166.
36. Kraysberg, Y.; Kudryavtseva, E.; McKee, A. C.; Geula, C.; Kowall, N. W.; Khrapko, K. Mitochondrial DNA Deletions Are Abundant and Cause Functional Impairment in Aged Human Substantia Nigra Neurons. *Nat. Genet.* **2006**, *38*, 518–520.
37. Chatterjee, A.; Mambo, E.; Sidransky, D. Mitochondrial DNA Mutations in Human Cancer. *Oncogene* **2006**, *25*, 4663–4674.
38. Ståhlberg, A.; Thomsen, C.; Ruff, D.; Åman, P. Quantitative PCR Analysis of DNA, RNAs, and Proteins in the Same Single Cell. *Clin. Chem.* **2012**, *58*, 1682–1691.